Growth of Carbon Nanotubes: A Combinatorial Method To Study the Effects of Catalysts and Underlayers

Hou T. Ng,*,† Bin Chen,† Jessica E. Koehne, Alan M. Cassell,† Jun Li,† Jie Han,† and M. Meyyappan

NASA Ames Research Center, Moffett Field, California 94035

Received: January 23, 2003; In Final Form: May 27, 2003

With their interesting electrical, structural, and physical properties, carbon nanotubes (CNTs) are envisioned to impact future nanoelectronics, nanosensors, and nanophotonics. Current research and development efforts in the growth of CNTs rely on the time-consuming one-parameter-at-a-time approach, whereby marginal variations in growth conditions from run-to-run experiments could result in substantially different outcomes. Here we report a highly efficient combinatorial approach to study the effects of catalysts and underlying metals for the generation of a comprehensive discovery library of CNTs. Shadow masking and sequential ion-beam deposition are used to construct an ensemble of catalysts and underlying metals on a generic addressable platform, whereby upon chemical vapor deposition, the CNT library can be assayed efficiently and conveniently to reveal a host of interesting phenomena. The approach could, in principle, be adapted and used for combinatorial investigations of other nanostructures.

Introduction

Carbon nanotubes (CNTs) show promise for applications in nanoelectronics, sensors, electrodes, and nanophotonics due to their unique electronic properties. These applications generally require controlled growth on patterned substrates. As a result, there has been a strong focus on using thermal and plasma chemical vapor deposition (CVD) techniques to realize CNT structures for these applications.[1−4] It is well-known that CNT growth by CVD requires a transition metal catalyst, and numerous studies have reported the use of Ni, Fe, Co, etc., with mixed results.[5] Consistent with the practice in the microelectronics industry, physical techniques such as sputtering or thermal evaporation are ideal to deposit the thin catalyst films. Though not always recognized, practical applications require a certain level of electrical conductivity which necessitates the use of a metal underlayer on the substrate beneath the catalyst.[2,3] In some cases, this metal layer can also act as a barrier layer to prevent the back diffusion of the catalyst. Again, there are several choices for the metal underlayer. There have not been any detailed studies comparing the effectiveness of various choices for the catalysts. Parametric study or optimization of any of the parameters, according to a survey of the CNT literature, was done[6,7] by the one-composition (or parameter)-at-a-time approach (i.e., a catalyst either with or without an underlayer) which is time-consuming and low in efficiency for discovering the optimum conditions. As a result, there is no direct comparison of various catalysts and various metal underlayers in their respective effectiveness. The present effort addresses this issue using a combinatorial approach.

Combinatorial approaches[8] have recently become popular both in the academic community and industry. They are high-efficiency, high-throughput methods, involving design and synthesis, to generate discovery "libraries" that can be systematically analyzed in parallel for specific properties of interest. The approach has been extensively used in the pharmaceutical and biotechnology industries with unprecedented success and has resulted in the rapid development of new drugs and genetic therapies.[9] Given this success, combinatorial techniques have attracted the attention of the materials community recently with the hope of discovering new materials with useful properties to meet future technological challenges and advanced applications. Significant discoveries have been documented, for example, in the development of novel functional dielectric, luminescent, superconductor, and magnetic materials.[10]

In CNT growth, Cassell et al.[11] pioneered the use of a combinatorial approach to identify optimum metal salt concentration along with structure-directing agents for growing multiwalled carbon nanotubes (MWNTs) and single-walled carbon nanotubes (SWNTs).[12] Note that solution-based catalyst preparation techniques are not amenable for growth on small patterns; more importantly, they involve numerous steps and are time-consuming.[5] In contrast, physical techniques for catalyst preparation such as ion beam sputtering, magnetron sputtering, etc., are fast and ideal for developing patterned growth processes. Here we report an innovative combinatorial approach to investigate the controlled growth of CNTs on a generic addressable platform, whereby the electrical and physical properties could be accessed to and probed efficiently and conveniently. Ion beam sputtering is used to deposit the catalysts and underlayers, and CVD is used to produce MWNTs. A matrix of catalysts and underlayers is investigated rapidly to identify effective combinations to meet application requirements.

Experimental Section

Rapid discovery of catalyst and metal underlayer schemes in a rational manner requires addressing the following needs: (i) approach to construct the combinatorial library, (ii) layout scheme of the addressable matrixes, and (iii) rapid characterization techniques to evaluate the results. We use a shadow masking

* Corresponding author. Phone: (650) 604 6146. Fax: (650) 604 5244. E-mail: hng@mail.arc.nasa.gov.

† Also at ELORET Corporation, Sunnyvale, CA 94087-4202.

10.1021/jp034198w CCC: $25.00
Published on Web 07/11/2003

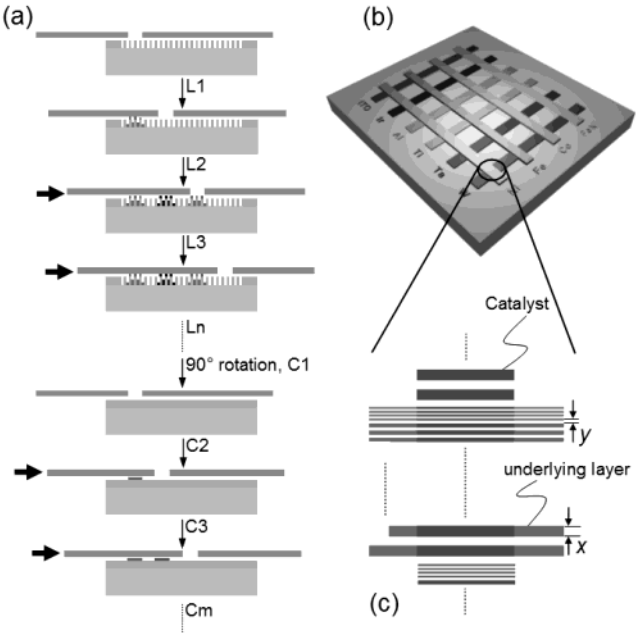

Figure 1. Fabrication scheme and the crossbar layout of the catalyst-underlying metal layer combinatorial library. (a) Sequential ion-beam deposition and a shadow masking technique were used to construct the library. The typical physical separation between the neighboring series was ~500 μm. (b) Perspective view of a cartoon showing the eventual combinatorial library prior to the CVD process. The elemental compositions that constitute the library are shown at the end of the lines. (c) An illustration showing the details at the intersection of the crossbar, with x ranging from 200 to 600 nm and y from 200 to 500 nm.

technique to introduce an ensemble of catalysts sequentially on a common supporting substrate. The synthesis and hence the CNTs are localized by maintaining a physical separation between the catalysts. In this approach, substrates with the potential to serve as device integration platforms such as single crystalline silicon, sapphire, silicon carbide, and silicon-on-insulator can be used, though the substrate choice is not one of the combinatorial variables in the present study. We also use an underlying metal layer scheme, forming a crossbar configuration with the catalyst, to achieve individual electrically addressable connections of the CNTs at each of the catalyst sites. There are two reasons for introducing an addressable array matrix as in Figure 1. First, it provides a means to investigate the effect of underlying metal layers on the growth phenomena of the CNTs. It has been reported that the structural and physical properties of the CNTs are highly influenced by the nature of the underlying metal layers under different growth conditions.[2,3,13] Second, it provides a means to explore the ability of the metals to serve as effective underlying conductive layers for electrical probing of the CNT−metal interfaces. As mentioned before, a good electrical conductivity (i.e., good ohmic contact) between the underlying metal layer and the CNTs is critical, besides the high quality of the CNTs, for the successful operation of electronic devices, electrodes, and sensors. Hence, the present crossbar layout should provide a useful means to consolidate relevant information on this aspect. The catalysts used are the following: iron (Fe), nickel (Ni), cobalt (Co), and a mixed alloy Fe/Ni; the candidates for the underlying layers include titanium (Ti), tantalum (Ta), aluminum (Al), tungsten (W), iridium (Ir), and indium tin oxide (ITO).

Figure 1 illustrates the fabrication scheme of the combinatorial library. Prior to the library construction, a UV-photolithography step was performed first to create an array of exposed windows with line widths (x) ranging from 200 to 600 nm and spacings (y) ranging from 200 to 500 nm. As shown by the process flow, a series of underlying metal layers (denoted as L1, L2, ..., Ln) were sequentially laid down by ion beam sputtering on a suitable substrate-of-interest, in this case a (100) silicon wafer, through a shadow mask. After deposition of the first series of L1, the shadow mask which was attached to a manual manipulator was moved to the next location to deposit the next series of L2 and so forth. The separations between each series of underlying layers could be controlled from several tens to hundreds of microns. Upon complete deposition of all the candidate underlying metal layers, the Si substrate was reorientated by a 90° rotation so that the opening slit of the shadow mask was orthogonal to the underlying layers. Ion beam sputtering was then used to fabricate a series of top catalyst layers (C1, C2, ..., Cm). The library construction was concluded with a final step involving the liftoff of the UV-resist. A typical crossbar layout of a completed combinatorial library is shown in Figure 1b. An expanded view of a crossbar reveals an array of individually addressable catalyst−underlying metal submicron lines (Figure 1c). Since submicron to nanometer length scale electrical contacts/interconnects are anticipated in future nanodevices, the inclusion of this parameter into the combinatorial matrix allows investigation of the dimensional effect on the growth phenomena and the structural integrity of the underlying layers upon subjecting to the high-temperature growth process. For the proof-of-concept experiment here, a shadow mask with a single opening slit was used. In principle, a shadow mask with strategically positioned multiple opening slits could be fabricated so as to achieve simultaneous copies of the complete library on a single substrate. After this, the substrate could be cleaved to obtain multiple copies which contain a complete library on each individual chip.

CVD was used to grow CNTs on the catalyst spots. Our apparatus and growth procedure have been described previously.[2,3] A feedstock of acetylene diluted in argon was used to grow MWNTs at temperatures of 750−900 °C. The variables considered to determine the optimal growth conditions include catalyst heat pretreatment time (t_1), the actual growth time (t_2), the growth temperature (T), and the flow rate (f) of carbon feedstock and carrier gas. Since the CNTs are localized in an array matrix, their structural characteristics and physical properties could be probed systematically by scanning the library platform using a series of characterization tools. The CNTs grown on all the spots of the library were first examined using scanning electron microscopy (SEM). A four-probe station linked to a semiconductor parametric analyzer was then used to obtain the two-terminal resistance at room temperature of each spot of the combinatorial matrix. Finally, high throughput Raman spectroscopy was also performed to examine each spot using 633 He−Ne and 785 nm diode laser excitations. The accumulation time used for each spectrum is 10 s. The micro Raman spectrometer scans through the CNT array matrix in micrometer steps, providing structural information with excellent spatial resolution. Further details can be found in ref 12. It is important to note that all three characterization schemes employed here, while providing useful information, are rapid to analyze the numerous combinations of the matrix.

Results and Discussion

Figure 2 shows an example of a collection of SEM images obtained after a thermal CVD process (t_1 = 10 min, t_2 = 5 min, T = 750 °C, f = 50 sccm). A quick glance at each of the intersection regions reveals either positive or no growth. The

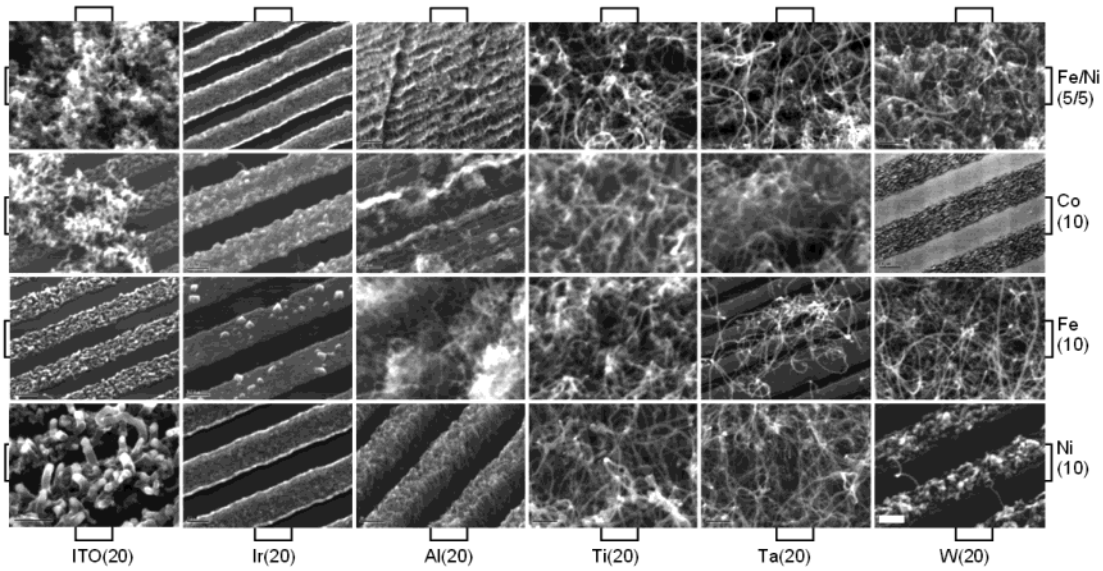

Figure 2. SEM perspective images (45° viewing angle) of CNTs grown from the combinatorial library of catalyst-underlying metal layers. The number in parentheses shown next to the elemental symbol indicates thickness (in nanometers) of the catalyst and underlying metal layer. The scale bar (= 500 nm) at the bottom left in the Ni/W panel applies to all panels as well.

TABLE 1: Various Structural Properties of Catalyst−Underlying-Metal-Layer Combinations

	ITO	Ir	Al	Ti	Ta	W	Si
FeNi	■ ◄ R H	■ ◄ R XL	■ ◄ R S XH	■ ◊ R XH	■ ◊ R H	■ ◊ R H	■ ◊ R XH
Co	■ ◄ R L	■ ◄ R XL	■ ◄ R H	■ ◊ R XH	■ ◄ R H	○	■ ◊ R XH
Fe	■ ◄ R XL	○	■ ► R H	■ ◊ R XH	■ ◊ R L	■ ◊ R XH	■ ◄ R XH
Ni	■ ► R H	○	■ ◊ R S H	■ ◊ R XH	■ ◄ R H	■ ◄ R XL	■ ◊ R XL

■ : multi-walled CNTs
□ : single-walled CNTs
○ : no growth
►: x ≥ 100nm (x: average diameter)
◊ : 50nm < x <100nm
◄: x ≤ 50nm

H : high density growth
L : low density
X : extreme high density
R : random (morphology)
S : regular array

general morphologies and structural dimensions of the CNTs were obtained by examining them at different magnifications. A summary of the structural properties, including the physical dimensions and morphologies at a submicron length scale, is tabulated in Table 1.

In general, it is observed that all metals, except Ir, could potentially serve as effective underlying metal layers for CNT growth with the appropriate catalyst selection. The growth on any catalyst−Ir combination was found to be sparse though Raman spectroscopy of these samples yielded all the appropriate peaks for MWNTs. In contrast, Ti, Ta (except Fe/Ta), and Al serve exceptionally well as underlayers for all the catalysts studied. With Ti, the diameter of the CNTs is typically between 50 and 100 nm and the growth densities are among the most consistent, regardless of the nature of the catalyst. The excellent wetting property of Ti is believed to be responsible by facilitating an even size distribution of the catalyst particles. With Ta and Al, a broader diameter range is generally noticed. In terms of the growth density, we found the highest on mixed alloy catalyst Fe/Ni with Al. The CNTs are so densely packed and organized in this case that only the top topography and the side walls of the CNT arrays could be imaged. Since Al has a lower melting point (660 °C) than Ti and Ta (1668 and 2996 °C, respectively), alloying with the catalyst is expected to occur to a larger extent leading to an increase in the number of reactive nucleating sites through surface clustering.[14] Nolan et al.[14] provide a rate equation for carbon deposition which explains the increased activity of a catalyst alloyed with a noncatalytic metal through the ability of surface clusters to increase the reactive sites. Except the growth on Ni/ITO, Ni/Al, and Fe/Ni/Al, we also observed the CNTs developing into highly intertwined networks. Among the catalysts used, we found the mixed alloy (Fe/Ni) to facilitate the most successful growth on the underlying layers in terms of density and quality. Among the CNTs, we observed those grown on Ni/ITO region to have the largest diameter (> 100 nm). In this case, the catalyst dots at the tip of the CNTs were identified by energy-dispersive X-ray analysis to be Ni, suggesting a tip growth mechanism. The ITO film essentially cracks at the growth temperatures and creates loose particles, which may be the reason for their presence at the CNT tips instead of at the base.

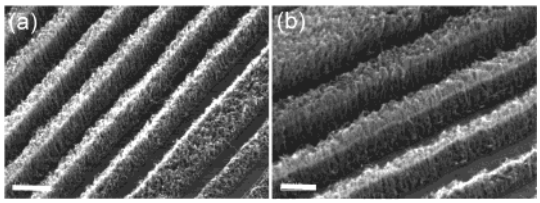

Figure 3. Thickness-dependent localized CNT arrays. (a) SEM image of localized CNT arrays on Ni/Al lines with increasing catalyst thickness (from right to left) from ~2 to ~10 nm. Scale bar: 1 μm. (b) SEM image of localized CNT arrays on FeNi/Al lines. The approximate thickness of catalyst is 5 nm. Scale bar: 500 nm.

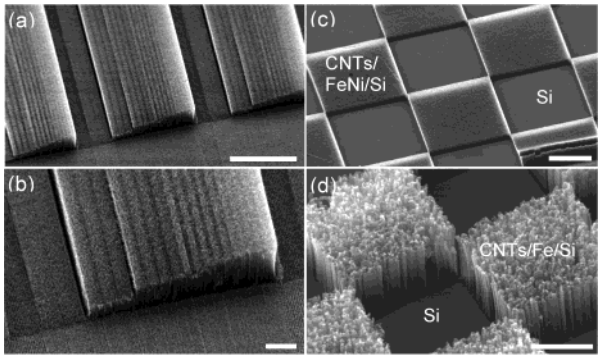

Figure 4. Stair-like and uniform CNT arrays. (a) A perspective SEM image showing highly regular CNT arrays on FeNi/Al submicron lines. Three stair-like CNT stripes are shown, suggesting highly organized assembly during the growth. Scale bar: 100 μm. (b) Close-up SEM image of the staircase, showing the progressive increase in the step height. Scale bar: 20 μm. (c) and (d) Regular checkerboards of vertically aligned CNTs with uniform height on FeNi/Si and Fe/Si, respectively. Scale bar: 100 μm.

From repetitive experiments, we found that a thickness in the range of 10−20 nm of the catalyst as well as the underlying metal layer serves well over an effective temperature range of 700 to 900 °C, in accordance with previous studies involving the one-composition-at-a-time approach.[3] Indeed, by taking advantage of the minimum opening gap between the shadow mask and the patterned Si substrate, we were able to create a thickness gradient of the catalyst at each intersection to investigate the effect of catalyst thickness on the CNT growth. As shown by the SEM images in Figure 3, consistent growth is generally initiated when a threshold catalyst thickness of ~2 nm is reached. In addition, highly localized CNT arrays could be observed, indicating the importance of the thickness parameter on directional organized growth. Figure 4 shows a striking example of the well-ordered CNTs presenting a staircase formation. The step height increases with decreasing x and y going from the left to the right, which we attribute to the increasing active catalyst surface area. We also notice the height of each step, corresponding to individual series of uniform x and y, to be rather consistent. The influence of the dimensional effect on such a formation is clearly seen when we compare CNTs grown on a larger scale and yet regularly patterned substrates (Figure 4c,d). In these cases, the straight sidewall profile of the arrays is evident from the SEM images, presumably due to the strong interaction among the CNTs during the growth. However, higher magnification images reveal the CNT arrays to be composed of nanotube bundles which grow upward while intertwining with their neighbors, in good agreement with previous reports.[1,3]

The effect of the flow rate (f) and the actual growth time (t_2) were observed to affect mainly the final physical length (l) of the nanotubes. In general, a larger f will result in smaller l, while the opposite holds for t_2 and l.

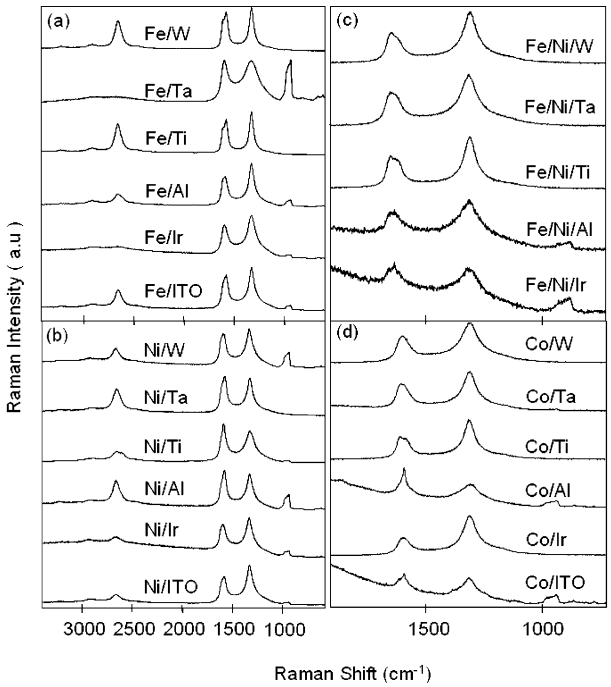

Figure 5. Raman spectra using 633 nm excitation (a and b) and 785 nm excitation (c and d).

High throughput Raman spectroscopy results (Figure 5) on the characteristics of MWNTs are discussed next. In general, most of the materials produced are MWNTs showing a high ratio of D-band (around 1332 cm^{-1}) to G-band (around 1585 cm^{-1}). In some cases, defective, fiberlike material was also seen, characterized by a shoulder at 1608 cm^{-1}. Small amounts of SWNTs were also seen under some conditions where metal oxides are detected in the Raman spectra; in these cases, a lower D/G ratio and sharper G-band features are seen. Figure 5 shows a sample of spectra among the numerous cases investigated. Iron catalyst with W, Ta, and Ti produces more disordered MWNTs (1608 cm^{-1}) than with Al, Ir, or ITO layers (Figure 5a). Ni catalyst produces predominantly MWNTs and less defective structures (1608 cm^{-1}) than Fe; in addition to MWNTs, a small percentage of SWNTs with Al, Ir, and ITO and defective MWNTs with W are seen. Figure 5c shows that the Fe/Ni alloy catalyst yields less defective MWNTs with good growth density. In Figure 5d, Co is observed to yield some SWNTs, especially with Al and ITO underlayers. In all the spectra, the peaks at 320 and 951 cm^{-1} are contributions from the silicon substrate; 1897, 2600 and 2700 cm^{-1} are SWNT secondary modes.

Carbon nanotubes are known to display either metallic or semiconducting properties.[15] Similar to aligned single-walled CNT bundles, MWNTs which consist of concentrically arranged cylinders are complex electrical conductors that incorporate many weakly coupled nanotubes, each exhibiting a different electronic structure.[16] Since a majority of the CNTs grown here are MWNTs, though some with defective structures as inferred from the Raman spectroscopy, electrically, a metallic behavior is anticipated. Indeed, we have used a four-probe station linked to a semiconductor parametric analyzer to investigate the equilibrium two-terminal electrical resistances at room temperature of the CNT combinatorial matrix. Figure 6 shows a series of typical current−voltage ($I-V$) measurements obtained from the matrix. Linear $I-V$ profiles are obtained for nearly all the

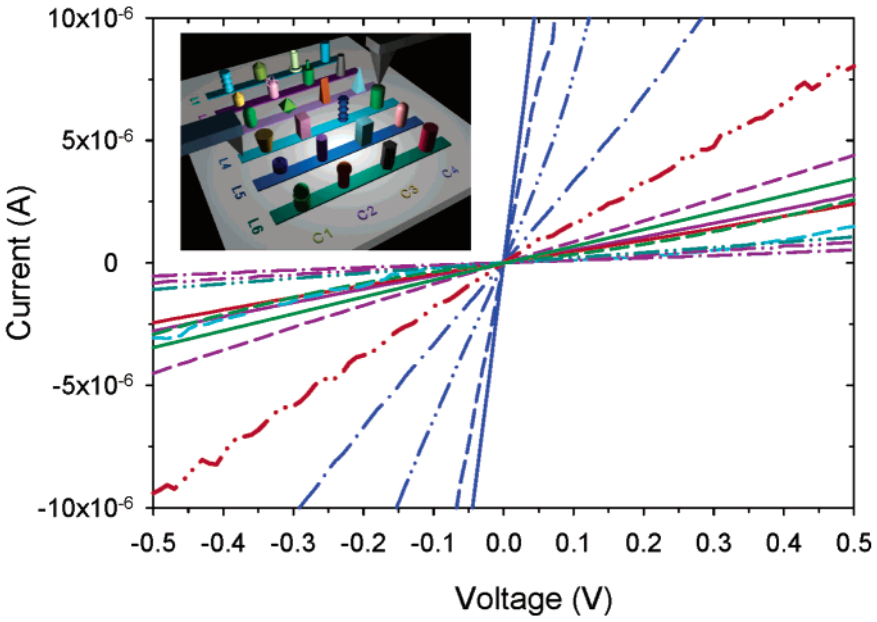

Figure 6. Two-terminal electrical resistance measurements of the CNT combinatorial matrix. $I-V$ curves were acquired at each of the crossbars with a four-probe station. The color legend is as follows: blue, Ti; red, W; dark pink, Ta; dark green, Al; cyan, ITO; solid line, Fe/Ni; dash−dot, Co; dash−dot−dot, Fe; and short dash, Ni. A schematic illustrating the probing of the CNT on underlying metals is shown in the inset.

CNTs, suggesting varying degrees of ohmic contact with the respective underlying metals. We observed low electrical resistances (∼4−30 kΩ) for MWNTs grown on Ti layers compared to higher resistances on all other underlying metal layers (∼57−1113 kΩ). The low end of this spectrum is with Al and Ta underlayers, whereas all the high resistances are with the ITO underlayer. The resistance with Ti is consistent with measurements obtained from MWNTs grown and processed using other techniques.[17] A better wetting capability and high melting point of Ti compared to other metals is believed to facilitate a better electrical contact with the CNTs. The intrinsic electrical resistivities of the metals, ordered Ta < W < Ti < Al < ITO, do not seem to dictate the observed results. $I-V$ measurements of the individual metal lines typically fall in the same order of magnitude as the CNTs. Since the probe has a relatively large radius (∼25 μm), we expect the electron transport to involve multiple bundles of CNTs. Although multiple shells could be in direct electrical contact with the underlying metal layers, electron transport is most likely to occur through the outmost shell since the probe is mainly in direct physical contact with the exterior of the nanotubes. Also, the absence of current saturation[15] with higher bias $I-V$ measurements further confirms insignificant contribution of charge transport within the CNTs. We also examined the structural integrity of the underlayers by exposing them to the growth conditions without the catalyst layers. As seen in Figure 7, there is no CNT growth. Small pinholes are observed on Al, otherwise the integrity of the metal lines is retained. The ITO lines exhibit significantly wide grain boundaries which may contribute to the slight nonlinear $I-V$ profile in Figure 6 for ITO.

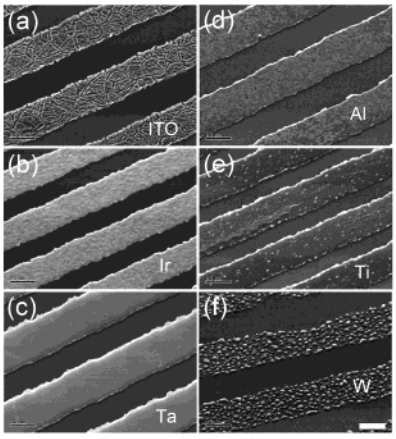

Figure 7. Structural morphologies of underlying metal layers. (a)−(f) SEM images of the underlying metal lines (without the catalyst layers) after subjecting to the entire growth cycle. No CNT growth is seen. Wide grain boundaries are observed in ITO lines while segregated clusters (∼50−80 nm) are found on W lines. Except for the minor pinhole formation (spiking) on Al lines, no significant morphological changes are observed on the others.

Concluding Remarks

We have presented a combinatorial approach for rapid investigation of catalysts and underlayers in the growth of carbon nanotubes. The study indicates Ti to be best among all the metal underlayers in terms of low contact resistance and high growth density. Among the catalysts, Fe/Ni and Ni seem to facilitate directional, organized growth on Al. In principle, the present approach can be extended to a host of other growth processes (such as plasma CVD) and nanostructured systems by appropriate selection of the active and supporting layers. The ease of this approach and customized characterization could potentially provide a new paradigm for advancing the fundamental understanding of structure−property relationships in the nanometer length scale regime. The approach also offers a possibility to shorten the time-to-discovery pathway whereby a potential exists for speeding up the innovative cycle, from discovery to bringing potential products to the market.

Acknowledgment. Work by ELORET authors was supported by a NASA contract.

References and Notes

(1) Fan, S.; Chapline, M. G.; Franklin, N. R.; Tombler, T. W.; Cassell, A. M.; Dai, H. *Science* **1999**, *263*, 512.

(2) Delzeit, L.; Chen, B.; Cassell, A. M.; Stevens, R.; Nguyen, C.; Meyyappan, M. *Chem. Phys. Lett*. **2001**, *348*, 368.

(3) Delzeit, L.; Nguyen, C. V.; Chen, B.; Stevens, R.; Cassell, A.; Han, J.; Meyyappan, M. *J. Phys. Chem. B* **2002**, *166*, 5629.
(4) Delzeit, L.; McAninch, I.; Cruden, B. A.; Hash, D.; Chen, B.; Han, J.; Meyyappan, M. *J. Appl. Phys.* **2002**, *91*, 6027.
(5) Meyyappan, M. In *Encyclopedia of Nanoscience and Nanotechnology*; Nalwa, H. S., Ed.; American Scientific Publishers: California, 2003.
(6) Hernadi, K.; Fonseca, A.; Nagy, J. B.; Siska, A.; Kiricsi, I. *Appl. Catal. A* **2000**, *199*, 245.
(7) Klinke, C.; Bonard, J. M.; Kern, K. *Surf. Sci.* **2001**, *492*, 195.
(8) *Handbook of Combinatorial Chemistry: Drugs, Catalysts, Materials*; Nicolaou, K. C., Hanko, R., Hartwig, W., Eds.; John Wiley & Sons: New York, 2002.
(9) *Integrated Drug Discovery Technologies*; Mei, H.-Y., Czarnik, A. W., Eds.; Marcel Dekker: New York, 2002.
(10) *MRS Bull.* **2002**, *27*, 4 and references therein.
(11) Cassell, A. M.; Verma, S.; Delzeit, L.; Meyyappan, M. *Langmuir* **2001**, *17*, 266.
(12) Chen, B.; Parker, G., II; Han, J.; Meyyappan, M.; Cassell, A. *Chem. Mater.* **2002**, *14*, 1891.
(13) Araki, H.; Kajii, H.; Yoshino, K. *Jpn. J. Appl. Phys.* **1999**, *38*, L1351.
(14) Nolan, D.; Lynch, D. C.; Cutler, A. H. *J. Phys. Chem. B* **1998**, *162*, 4165.
(15) *Carbon Nanotubes: Synthesis, Structure, Properties & Applications*; Dresselhaus, M. S., Dresselhaus, G., Avouris, P., Eds.; Springer-Verlag: New York, 2001.
(16) Collins, P. G.; Arnold, M. S.; Avouris, P. *Science* **2001**, *292*, 706.
(17) Li, J.; Stevens, R.; Delzeit, L.; Ng, H. T.; Cassell, A.; Han, J.; Meyyappan, M. *Appl. Phys. Lett.* **2001**, *81*, 910.